www.czasopisma.pan.pl PAN POLSKA AKADEMIA NAUK www.journals.pan.pl

Arch. Min. Sci. **70** (2025), 2, 163-181

Electronic version (in color) of this paper is available: http://mining.archives.pl

DOI: https://doi.org/10.24425/ams.2025.154657

LESZEK SZOJDA[1*], BERNARD KOTALA[1]

BEHAVIOURAL ANALYSIS OF A RESIDENTIAL BUILDING SUBJECTED TO INFLUENCES OF DISCONTINUOUS GROUND DEFORMATIONS: CASE STUDY IN THE UPPER SILESIA, POLAND

The end of the long-term exploitation of minerals makes it possible to stop maintaining underground infrastructure and pumping out water. This raises the groundwater table and may cause changes in the mechanical parameters of the subsurface soil layers. The occurrence of these phenomena in urban areas has raised concerns about the safety of residential buildings subject to such influences. The analysed two-storey building, without a basement, had a square plan and a typical brick wall structure with RC structural elements: foundation strips, inter-storey ceilings, ring beams on load-bearing walls and stairs. The numerical model also included the groundmass to consider the soil-structure interaction effect. During the calculations, all loads occurring during the standard operation of the building and two locations of the sinkhole under the building's foundations were considered. The results of the analyses are presented in the form of colour maps showing the displacement of the building, the change in stresses in the soil under the foundations, the change in the principal stresses in the building structure and the possibility of cracks appearing. The analyses show that the building will not be destroyed, but there will be damage to the load-bearing walls.

Keywords: Discontinuous ground deformations; FEM numerical analysis; soil-structure interaction; brick wall structure

1. Introduction

The underground exploitation of minerals causes environmental changes and surface deformations, which have been widely described [1-4]. Depending on various factors, ranging from natural factors (such as the arrangement of subsoil layers and rock mass discontinuities) to the method of mineral exploitation, subsoil deformations occur on the ground surface. Predictions

[1] SILESIAN UNIVERSITY OF TECHNOLOGY, DEPARTMENT OF STRUCTURAL ENGINEERING, 5 AKADEMICKA STR., 44-100, GLIWICE, POLAND

* Corresponding author: leszek.szojda@polsl.pl

of their occurrence became the basis for the development of many methods of subsidence forecasting [1-3,5-10]. At the same time, methods were developed to monitor surface deformations [2,11-14] and minimise their impact [15-17]. Buildings located in such areas are subject to additional impacts which, depending on their intensity and the resistance of the structures, may lead to significant damage or destruction of the structure [18]. New methods for predicting damage to buildings subjected to continuous deformations have been presented in [19,20], but they are not yet applicable to discontinuous deformations. This became the basis for developing methods of protecting structures against the impact of discontinuous deformations [21-25]. In the 20th century, this also allowed the adoption of a set of facility design instructions issued by the Building Research Institute in Warsaw, Poland [26,27]. The situation in the case of discontinuous deformations is much less favourable. Discontinuous deformations, in the form of local ground displacements, appear randomly and, despite the existing methods of predicting their occurrence [28,29], pose significant threats to objects. Determining the behaviour of objects affected by such influences should account for the soil-structures interaction (SSI) [30,31].

Hard coal exploitation in Upper Silesia is slowly being limited by the policy adopted by the authorities [32]. However, cessation of exploitation involves other threats. The occurrence of discontinuities in the rock mass, in the form of faults [3,33-35], as well as the abandonment of the use of excavations and the cessation of pumping out of the water, resulting in the disclosure of discontinuous deformations [36,37]. The rising groundwater levels up to the ground surface cause changes in the ground parameters of the subsurface layers. In the case of shallow mining carried out in the past (up to 100 m below ground level), this may result in the activation of old post-mining voids and reveal discontinuous deformations, in the form of sinkholes, in areas previously considered suitable for development. Buildings in these areas have been protected against continuous (milder) deformations. However, the occurrence of discontinuous deformations, which are difficult to locate, prompted the authors of this study to perform a numerical analysis of a building which may be subject to the influence of discontinuous deformations, i.e. the collapse of part of the ground underneath the foundations. The problem is current, from the point of view of surface development in areas of mine cessation in many regions of Upper Silesia. It can also be related to similar regions and impacts on similar buildings.

2. Description of the considered case

2.1. Mining situation

The area around the building being studied used to have mining activities in previous centuries. Five coal seams were mined to a depth of 300 m below ground level. TABLE 1 displays the mining depth, wall thickness, duration, and location in relation to the facility. Fig. 1 shows an outline of the location of the shallowest exploited seam, in relation to the building. Most seams were exploited by filling the resulting spaces with sand (so-called ‘hydraulic backfilling’). Only the shallowest seam has no information concerning how it was mined, due to the fact it was extracted in the first half of the 19th century.

The mine which exploited deposits in this area was closed in 2001. Later, other nearby mining plants were also closed, and the maintenance of mine workings and galleries was stopped, including the cessation of the mine water pumping. This led to a rise in the groundwater table, which, in turn, caused a change in the equilibrium state of the subsurface soil layers. Currently,

TABLE 1

Mined coal seams whose impact affected the location of the building

	Depth of exploitation [m b.g.l.]	Thickness of the coal seam [m]	Operating time [years]	Method of operation
1.	22.5	4.20	1808-1852	unknown
2.	86.4	4.20	1955-1956	hydraulic backfilling
3.	121.8	2.00	1958	hydraulic backfilling
4.	148.1	2.70	1957-1958	hydraulic backfilling
5.	230.0	2.40-2.85	1976-1977	hydraulic backfilling
6.	250.0	2.80-3.00	1978	hydraulic backfilling
7.	280.0	2.00	1985	hydraulic backfilling

the workings of the shallowest coal seam, which were not filled during the hydraulic backfilling process, appear on the ground surface in the form of sinkholes. The locations of recently formed sinkholes are shown in Fig. 1.

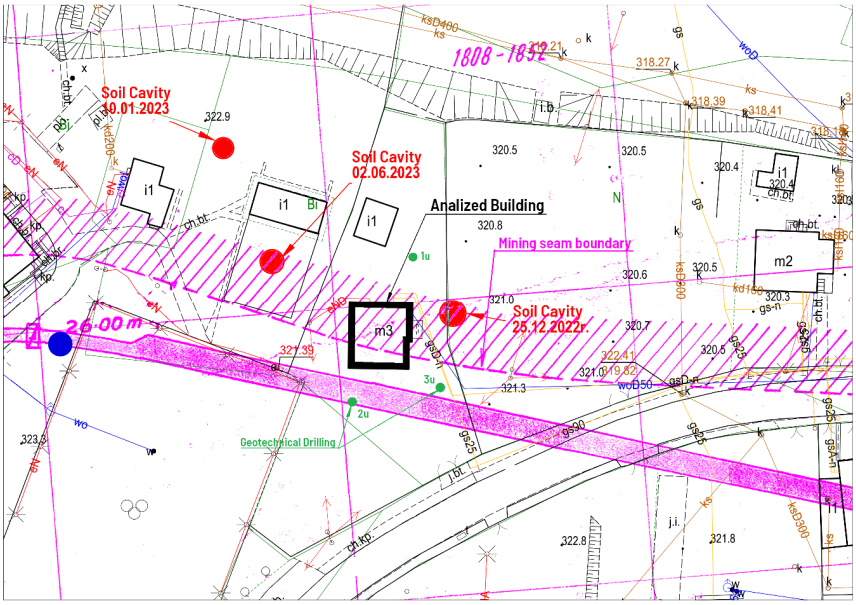

Fig. 1. Location of the analysed building against the background of the shallowest exploited seam with the places and dates of the sinkholes [38]

Since 2005, several radar, gravimetric and microgravimetric measurements have been carried out to determine the risk of sinkholes in the area of the building. The research showed that the occurrence of a sinkhole in the building area is possible with a certain probability. Additionally, the location of the sinkhole cannot be precisely determined due to the heterogeneous structure of the ground. This was the reason for carrying out a numerical analysis of the impact of typical sinkholes on the facility.

2.2. Description of the structure

The building in question was designed and constructed in the 1980s after deformations caused by previous use were revealed. Consistent with the design guidelines, the building was protected against the effects of continuous terrain deformations. The main strengthening elements were appropriately designated: reinforcement of foundation strips, diagonal ties, and reinforced concrete (RC) ceilings with ring beams placed on load-bearing walls.

The building has a plan area similar to a square, with external dimensions of 10.50×11.05 m; there is no basement, there are two floors above ground and an unused attic. The foundations of the building were placed approximately 90 cm below ground level, and they consisted of RC foundation strips under the external and two internal walls, 35 cm thick and 80 and 60 cm wide, respectively. Diagonal ties were placed at the foundation level, with a cross-section of 40×35 cm. The foundation strips and diagonal ties were reinforced with 4ϕ16 steel bars with a yield strength $Q_r = 2500$ kG/cm^2, which corresponds to steel grade A-I ($f_{yk} = 240$ MPa) and made of concrete $R_w = 140$ kG/cm^2, which corresponds to today's class of concrete between C12/15 ($f_{ck} = 12$ MPa) and C16/20 ($f_{ck} = 16$ MPa). The foundation walls of the building were made of concrete $R_w = 140$ kG/cm^2 and had strip widths based on the design.

The load-bearing walls of the above-ground floors were made of solid brick and aerated concrete (FGS – foam-gas-silicate) with a thickness of 40 cm (with plaster). The partition walls of the rooms were made of 15 cm thick brick (with plaster). The ground floor and first floor were closed with monolithic RC slab ceilings, 8.5 cm thick, and with a concrete strength of $R_w = 140$ kG/cm^2. The reinforcement of the slabs was made of steel with a yield strength $Q_r = 2500$ kG/cm^2 and were bars with a cross-section depending on the span, in the range from ϕ8/25 cm to ϕ10/12.5 cm. Loads from the ceiling slabs were transferred to the walls using RC rings, arranged circumferentially on all load-bearing walls. The class of steel and concrete of the ring beams was the same as that of the ceiling, and the reinforcement cross-section was 4ϕ16. Vertical communication was provided by slab stairs made of RC, with the same material parameters as for the ceilings.

The building's roof was a hipped wooden roof with a rafter-purlin structure. The rafters were based on peripheral walls and purlins located approximately halfway along the rafter length. The roof covering was a steel sheet in the form of tiles. A general view of the building is shown in Fig. 2.

Three geotechnical boreholes ('1u' to '3u', Fig. 1) were drilled around the building and found that it was founded on a layer of medium sand (MSa) with a thickness of 3.5-5.0 m below the foundation level. Below this was a layer of compact clay (MCl) to a depth of more than 10 m. The values of the mechanical parameters of these layers are shown in TABLE 2.

Fig. 2. General view of the building from the north-east and south-east (source: authors' own materials)

TABLE 2

Physico-mechanical parameters of the ground under the building, according to [39]

Ground	Internal friction angle ϕ [°]	Cohesion c [kPa]	Compressibility modulus M_o [MPa]	Specific density γ [g/cm^3]
Medium Sand (MSa)	38.0	0.0	100	1.80
Medium Clay (MCl)	20.0	30.0	50	2.10

3. Numerical model of the soil-structure interaction

Numerical analyses were carried out using a numerical software package ATENA (*Advanced Tool for Engineering Nonlinear Analysis*) version 5 (processor) [40]. However, the building model was built using CAD-type programs and GiD (pre-processor) version 13.4, in which the material models of the ATENA processor were implemented.

3.1. Geometry and structural model of the building

To accurately assess the effect of the deforming ground on the structure, soil-structure interaction (SSI) analysis was utilised. This solution is advisable if the mechanical properties of the materials are different, and the interactions of these materials may cause non-elastic phenomena in the system. The analysed case included a model of the building structure and the soil volume to a depth of 10 m below the foundation level. This made it possible to reflect the mutual influence of both centres in the most realistic way.

The building structure was analysed without accounting for the wooden roof structure, which did not significantly affect the stiffness of the remaining part of the building. Fig. 3 shows a general three-dimensional model of the building, with elements of the roof structure to illustrate the whole.

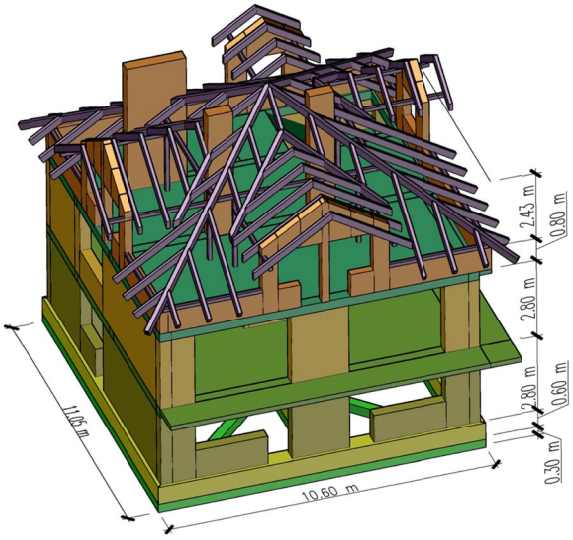

Fig. 3. 3D model of the building prepared for analysis: view from the south

3.2. Soil material model

To take into account SSI and the inability to determine the displacements of the area loaded with the structure as a result of mining deformations (especially discontinuous ones), the solid ground on which the building was founded was modelled. In the numerical analysis, the arrangement of layers of the modelled soil volume was reproduced following the test results obtained from geotechnical drillings [38], as presented in TABLE 2. The numerical analyses used a material model based on the assumptions of the 'Drucker-Prager' theory [41,42], implemented in the ATENA program. The required parameters describing this model are presented in TABLE 3. The numerical model of the building, together with the ground structure, is shown in Fig. 4. The

TABLE 3

Fundamental soil characteristics based on the material model implemented in the ATENA software

Feature	Medium Sand (MSa)	Medium Clay (MCl)
• Internal friction angle	38.0°	20.0°
• Cohesion	0.00 MPa	0.03 MPa
• *Young's* modulus	100.00 MPa	50.00 MPa
• *Poisson* ratio	0.20	0.20
• Angle of inclination of the surface *Drucker-Prager* cone	0.298	0.149
• *Drucker-Prager K* parameter	1.145 kPa	36.741 kPa
• Limit displacement in compression (plasticity property of soil in compression)	–0.030 m	–0.050 m
• Volumetric weight	18.0 kN/m^3	21.0 kN/m^3

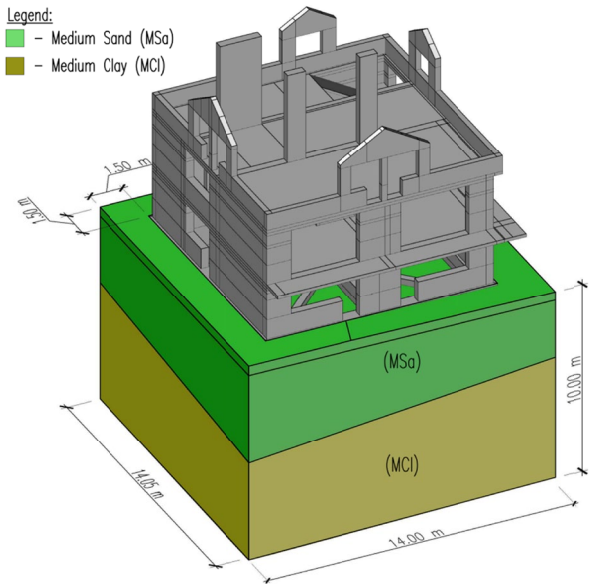

Fig. 4. View of the numerical model with a soil block of assigned soil material characteristics: MSa – medium sand, MCl – medium clay

ground volume is limited by planes on the sides and bottom of the model. All finite elements with nodes located on these planes were prevented from moving in the direction perpendicular to each plane (*X*, *Y* and *Z*, respectively).

3.3. Material model of the structure

The basic structural materials presented in Section 2.2 were adopted in the numerical analysis. For brick and concrete elements, the analyses were carried out using material models available in the software library under the name '*Concrete EC2: CC3DNonLinCementitious2*', which uses a boundary surface based on the Willam-Warnke relations [43,44]. Masonry walls were modelled using the finite element method for a homogeneous material with averaged strength parameters [45,46]. For the RC elements, a model available in the software library under the name '*Reinforced Concrete: CCCombinedMaterial*' was used. This model combines the material models of concrete and steel, but the reinforcement is treated as blurred. The effect of 'blurring' the reinforcement was achieved by assessing the extent of reinforcement in a specific direction of the reinforcing bar arrangement. The main characteristics of the material models used are presented in TABLE 4; Fig. 5 shows the numerical model with the assigned materials.

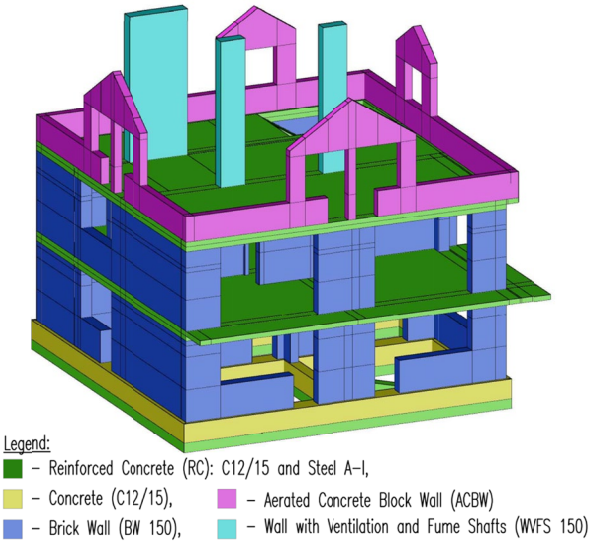

Fig. 5. View of the numerical model with assigned materials (designations according to TABLE 4)

3.4. Model contact layers

To ensure proper cooperation between the structure and the ground and to simulate the sinkhole, a contact layer (interface) was modelled, enabling proper interaction between various material media. The contact layer was introduced in the form of the so-called 'zero volume' between the strip footings and foundation walls and the ground and between the solid mass of soil and the part subject to displacement (Fig. 6). The task of the contact layer is to only transfer

TABLE 4

List of basic features of material models

Material feature for the markings in Fig. 5	Concrete (C12/15) [47]	Steel (A-I) [47]	Brick wall (BW 150) [47-49]	FGS wall (ACBW) [47-49]
• Compressive strength	12.0 MPa	—	2.2 MPa	3.5 MPa
• Tensile strength (yield strength for steel)	1.10 MPa	210.0 MPa	0.22 MPa	0.50 MPa
• Tensile strength (ultimate strength for steel)	—	240.0 MPa	—	—
• Modulus of elasticity	27.0 GPa	200.0 GPa	1.1 GPa	2.2 GPa
• Poisson ratio	0.2	—	0.2	0.2
• Fracture energy	2.75E-05 MN/m	—	4.00E-05 MN/m	2.00E-05 MN/m
• Plastic strain	–0.0013274	—	–0.0020000	–0.0015900
• Critical displacement in compression	–0.0005 m	—	–0.0005 m	–0.0005 m

compressive or shear forces (friction) to the modelled soil body, omitting the forces causing tensile stresses in the soil. Thus, in places where tensile stresses occur, the contact layer is intended to enable the foundation to detach from the ground, as well as to enable the collapsing soil to detach from the remaining part without causing additional stresses. The parameters of the contact layers, determined based on the guidelines provided in [40], were applied to the material model of the contact layer, implemented in the software package, and presented in TABLE 5.

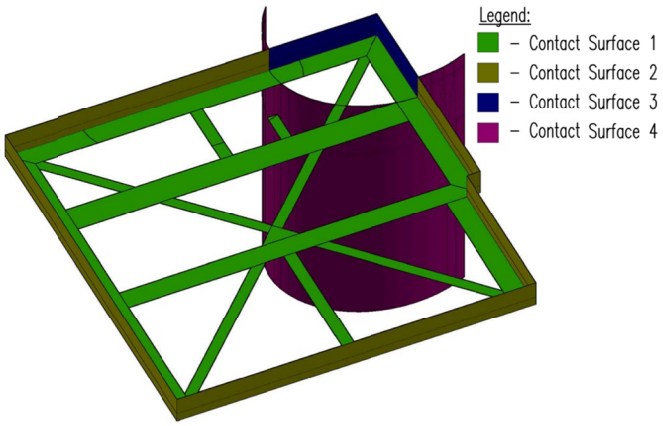

Fig. 6. View of the contact surface location: 1 – between the bottom of the footings and the ground; 2 and 3 – between the side of the footings and foundation walls and the ground; 4 – between the solid block of soil and the sinkhole

3.5. Applying loads to the object and the ground

To determine the impact of the deforming ground on the building, it was necessary to obtain a state of stress in the building at which sinkholes could occur. For this reason, so-called program

TABLE 5

Summary of the strength parameters of the contact surface

Strength characteristic	Contact Surface (Fig. 6)		
	1 and 2	3	4
• Normal stiffness (under compression)	1,0E+04MN/m^3	1,0E+04MN/m^3	1,0E+04MN/m^3
• Tangential stiffness (under shear)	1,0E+03MN/m^3	1,0E+03MN/m^3	1,0E+03MN/m^3
• Cohesion	1,0E-03kPa	1,0E+00kPa	3,0E+01kPa
• Friction coefficient	1,0E-06	1,0E-03	1,0E-03
• Tensile strength	1,0E-03kPa	1,0E+00kPa	1,0E+00kPa
• Minimum normal stiffness (under compression)	1,0E+02MN/m^3	1,0E+02MN/m^3	1,0E+02MN/m^3
• Tangential stiffness (under shear))	1,0E+01MN/m^3	1,0E+01MN/m^3	1,0E+01MN/m^3
• Ability to displace the contact layer	No	Yes	Yes

loads (self-weight, live loads, snow and wind effects) were applied in the initial phase, with parts of the ground removed accordingly in the next phase.

An operational situation was assumed for quasi-constant load values in the first part of the loading. For the analysis, it was assumed that the operational loading occurred on all surfaces of the ceilings and stairs but only up to the value of the long-term variable load. The basic load values considered in the quasi-static load combination are presented in TABLE 6.

TABLE 6

Summary of basic program loads for the analysed building

No.	Load description	Characteristic load value [kN/m^2]
1.	Permanent load from the roof covering	0.575
2.	Equivalent permanent load transferred from the roof surface to the ceiling	0.515
3.	Equivalent permanent load transferred from the roof surface to the wall cross-section area	6.046
4.	Permanent load of a typical floor	1.079
5.	Load of foundation ties with backfill soil and floor on the ground	12.647
6.	Self-weight of the modelled building elements – automatically added in the calculation software	
7.	Variable live load (limited to the value of the long-term live load)	0.6
8.	Variable load from wind effect – omitted in the analysed quasi- constant combination	
9.	Variable load from snow effect – omitted in the quasi- constant combination	

The second type of load is related to moving ground, imitating the formation of a sinkhole. From the previous observations of the area presented, it was found that the sinkholes occurring in this area have a shape similar to a circle, with diameters not exceeding 6.0 m. The depth was usually specified as being several metres. The walls of the sinkhole had an almost vertical slope. When identifying the location of the building near the exploited seam (Fig. 1), it is clear that

it is situated on the edge of the selected deposit. For this reason, it was assumed that the most likely location of a possible sinkhole affecting the facility may appear near its northern wall. This was the reason for considering two positions of the sinkhole in relation to the object (Fig. 7). It was assumed that, in each position, the edge of the sinkhole would be vertical, and the vertical displacement would be 3.0 m.

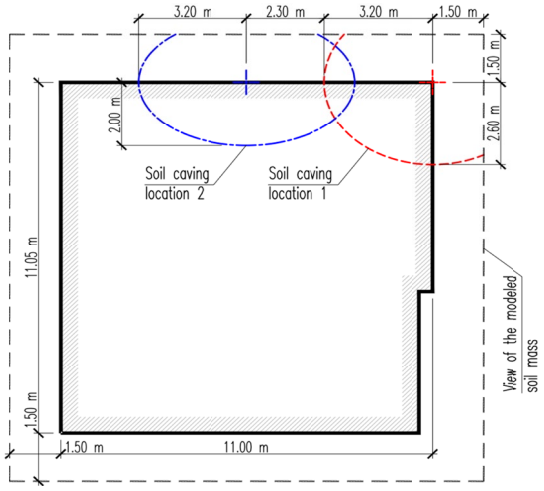

Fig. 7. Building plan: Location and general dimensions of the modelled sinkholes

To accurately reproduce the behaviour of the object, loads should be applied gradually to avoid significant deformations when the load capacity of the structural elements modelled by finite elements is exceeded. Load intervals were used here and were divided into appropriate calculation steps. The following load application method was used:

- Interval 1: checking the structural model, including boundary conditions (load step 0);
- Intervals 2-5: application of self-weight, permanent and variable loads (load steps 1 to 40);
- Intervals 6-9: vertical displacement of the soil mass by 3.0 m (load steps from 41 to 355).

During the analysis, up to 100 iterations were carried out in each computational step, which allowed for the convergence of solutions during the analysis. The Newton-Raphson [40] method was applied, and a convergence criterion of 1% was assigned for the displacement, residual force and absolute residual force error, while a 0.01% criterion was assigned for the energy error.

3.6. Division of the numerical model into finite elements

The numerical model used finite elements with a tetrahedral shape (tetrahedral structural mesh) and a prismatic shape for the contact layers, characterised by zero thickness (zero volume). They were finally divided (according to the location of sinkhole 1/2) into:

- 155 057/156 066 – tetrahedral volume elements,
- 5 617/6 037 – prismatic volume elements,
- 46 390/46 872 – nodal points.

An example of the numerical model divided into finite elements is shown in Fig. 8.

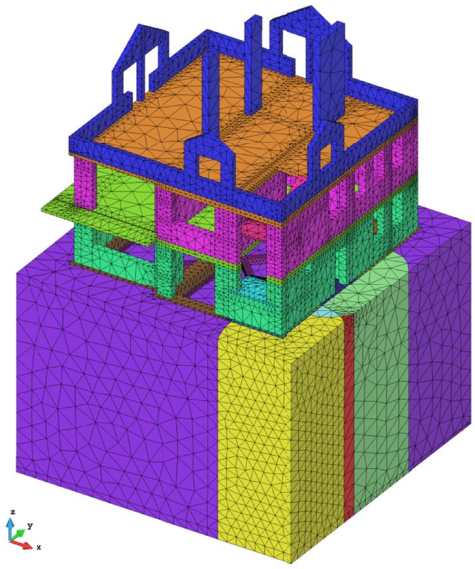

Fig. 8. View of the numerical model divided into finite elements, for example, for a model with the location of sinkholes in the ground

4. Results of numerical analysis

The behaviour of the building structure subjected to discontinuous deformations was analysed in several steps and on several levels. The analyses were carried out in the following areas:

- Vertical displacements of the structure (X_3) caused by the sinkhole;
- Changes in vertical stresses σ_{zz} in the ground under the building's foundations;
- Changes in principal tensile stresses σ_{max} in the building structure;
- Possibility of cracks appearing in the northern and eastern parts of the building.

These results were presented for each of the two analysed locations of the sinkhole relative to the building. The presented results can be shown in the following load states (Figs. 9-11 and 13-15):

(a) Full program load of the structure (step 40);
(b) Vertical ground displacement of –27.5 cm (step 135);
(c) Vertical displacement of the ground to the level of –100 cm (step 230);
(d) Vertical displacement of the ground to the level of –300 cm (step 355).

4.1. Sinkhole in position 1

The location of sinkhole 1 includes the smallest area of loss of support for the building's foundations. This occurs in the north-eastern corner and causes the cantilevering of the corner of

the structure. The vertical displacement (X_3) of the structure and the soil mass of the sinkhole in location 1 are shown in Fig. 9. It should be noted that the structural displacement values increase when the bottom of the sinkhole is significantly below the bottom of the foundations.

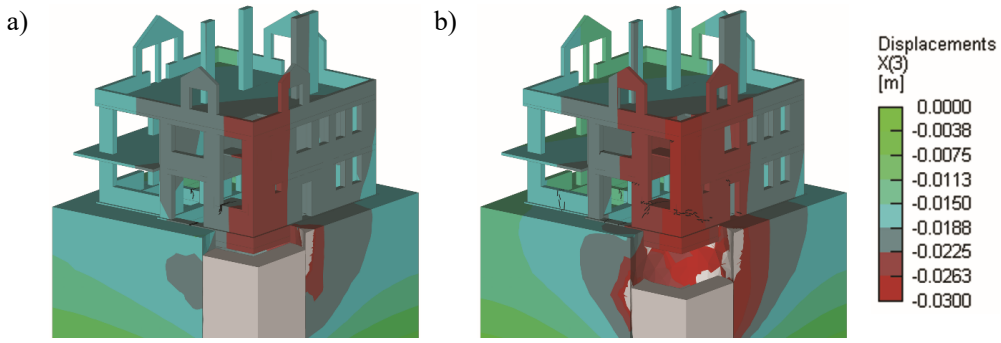

Fig. 9. Vertical displacements of the building structure in subsequent numerical steps (north-east corner): a) step 230; b) step 355 – deformation scale x1'

The largest corner displacements reach a value of 3 cm, which, for a building diagonal with a length of approximately 14.5 m, gives an average floor inclination of approximately 2‰.

The changes in vertical stresses in the ground under the foundations allow the observation of the use of the load-bearing capacity of the ground elements. Fig. 10 shows the vertical stresses σ_{zz} and clearly shows that, in the case of program loads (Fig. 10a), the stresses in the substrate are relatively equal and do not exceed 80 kPa. In the subsequent steps of removing the support, an increase in stress can be seen at the edges. With significant vertical displacements, a decrease in vertical stresses in the ground in the corner opposite to the sinkhole and significant increases in stresses in the upper right corner and halfway along the wall are visible (Fig. 10b). At the very edge of the sinkhole, the stresses in the subsoil decrease due to the possibility of deforming the soil horizontally, towards the resulting void.

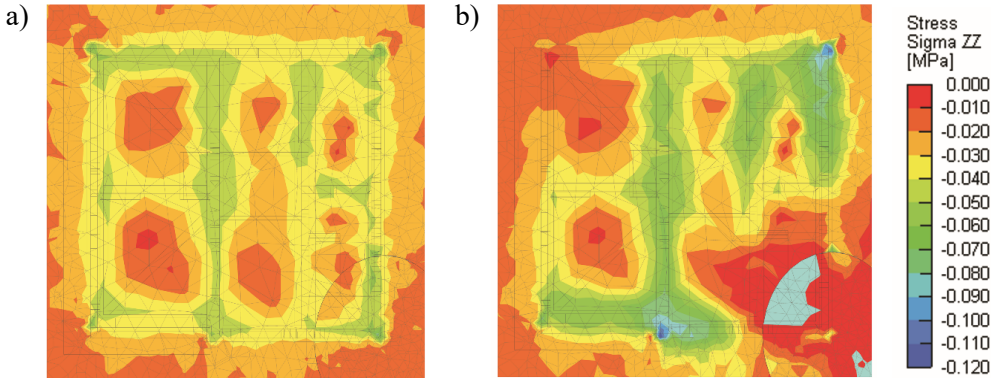

Fig. 10. Vertical stresses σ_{zz} in the soil under the foundation strips of the building in the following calculation steps: a) step 40; b) step 355

The main tensile stresses σ_{max} are shown in Fig. 11. They are responsible for the possibility of cracks occurring in structures made of traditional materials.

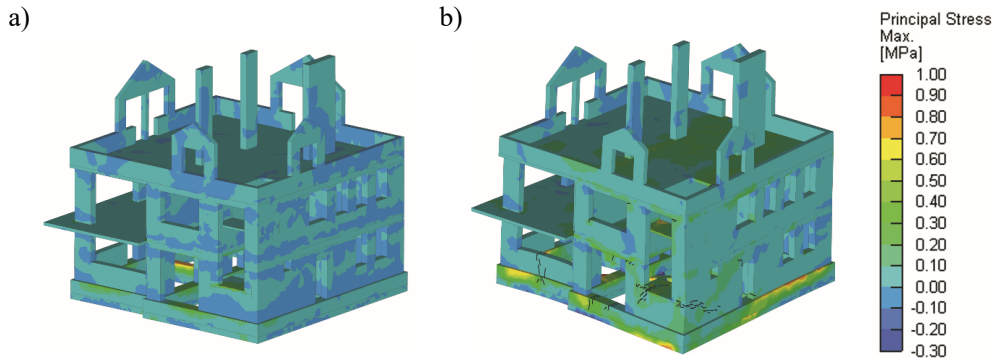

Fig. 11. Principal tensile stresses σ_{max} in the building structure (north-east corner) in the following calculation steps: a) step 40; b) step 355 – deformation scale ×100'

As the loads and deformations of the system increase, damage in the form of cracking appears. Fig. 12 shows the location and probable crack width for the last calculation step. It should be noted that the weakest elements (made of brick) and the concrete elements are damaged. RC elements that strengthen the structure are not cracked.

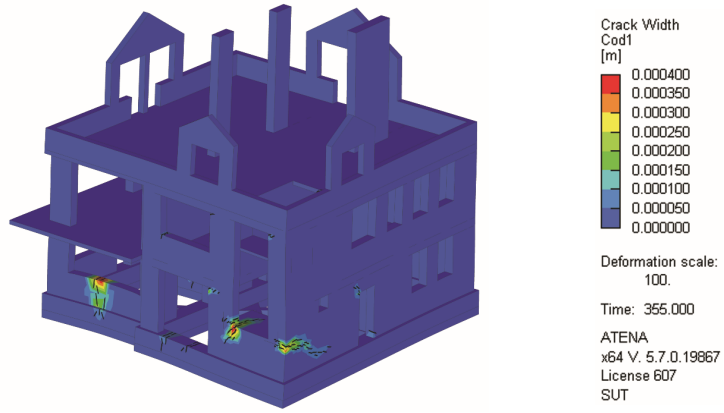

Fig. 12. Structural cracking of the building (north-east corner) in the 355th calculation step: deformation scale ×100 and the crack width is shown from 0.1 mm

4.2. Sinkhole in position 2

The location of sinkhole No. 2 only covers the northern wall of the building. The foundation loses support for about 6.4 m, and this part of the structure begins to function like a tall beam or deep beam. The vertical displacements of the entire system are shown in Fig. 13.

In this case, the vertical displacements X_3 are the same in value but cover the entire width of the northern wall. A displacement of –3.0 cm along the length of the building's side (for 11.5 m) causes the floors to slope by approximately 2.6‰.

The vertical stresses σ_{zz} under the footings are shown in Fig. 14. As in the previous case, stress redistribution occurs when the ground displacement (bottom of the sinkhole) is relatively deep. Then, the ground elements at the edge of the sinkhole can deform, and stresses are reduced. Greater stresses occur in more distant elements and under the internal walls (Fig. 14b). The stresses in the wall opposite the sinkhole drop significantly, which is also confirmed by the slope of the terrain.

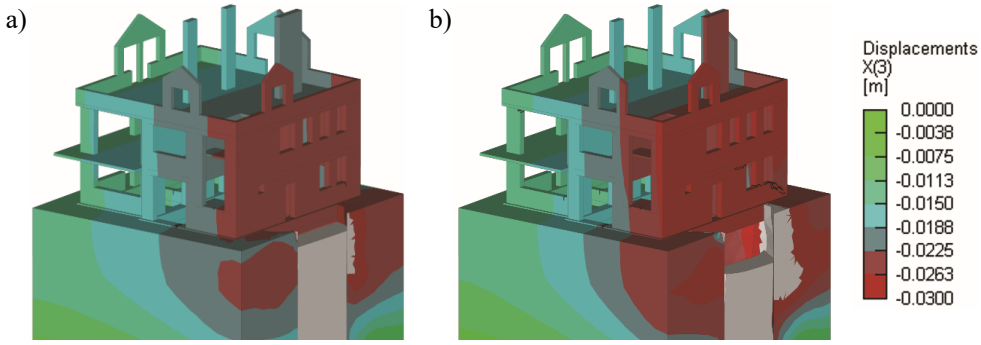

Fig. 13. Vertical displacements of the building structure in subsequent calculation steps (view of the north-east corner): a) step 230; b) step 355 – deformation scale ×1'

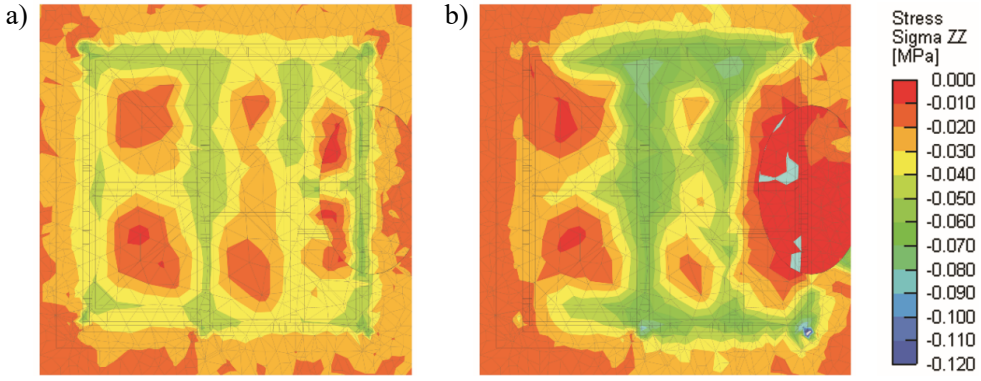

Fig. 14. Vertical stresses σ_{zz} in the soil under the foundation strips of the building in the following calculation steps: a) step 40; b) step 355

The principal stresses are also redistributed. Their distribution, in selected calculation steps, is shown in Fig. 15. Stress concentrations occur in the foundation elements (Fig. 15b) due to the spatial operation of the entire structure. The level of these stresses is not so high that it will cause damage to the RC foundation.

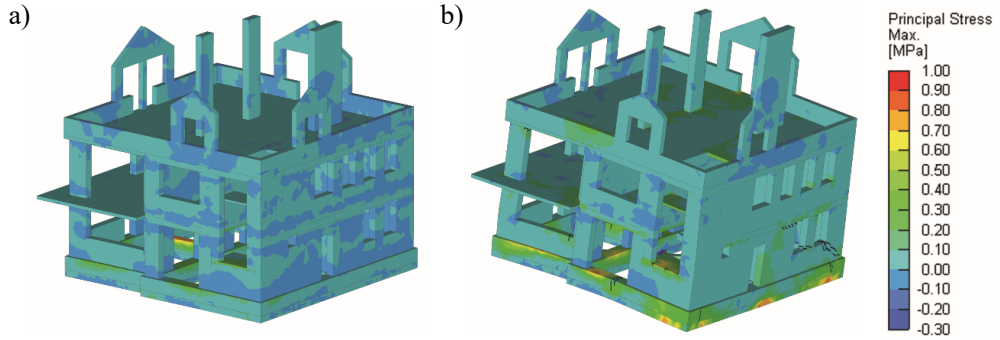

Fig. 15. Principal tensile stresses σ_{max} in the building structure (north-east corner) in the following calculation steps: a) step 40; b) step 355: deformation scale ×100

The structural cracking shown in Fig. 16, in the last calculation step, appears in places with the greatest use of materials. The brick wall in the northwest corner is visible under the ground floor window due to the bending of the wall structure, which follows the settling ground. The second crack in the underground part of the eastern wall is in a significantly weakened section due to the entrance openings.

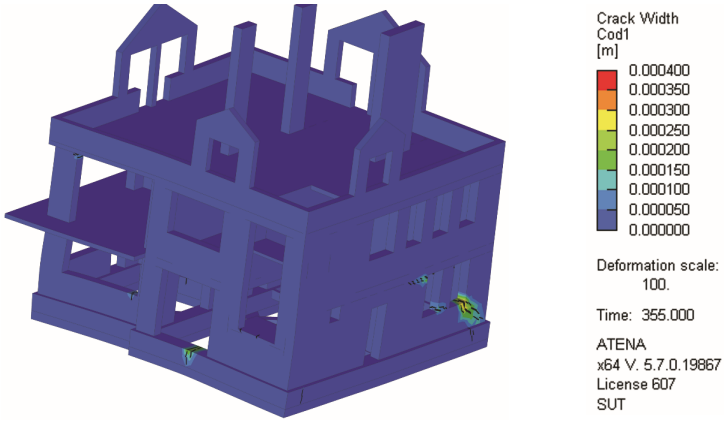

Fig. 16. Structural cracks of the building (north-east corner) in the 355th calculation step at a deformation scale ×100; the width of the cracks is shown from 0.1 mm

5. Summary and conclusions

The study aimed to assess the behaviour of a residential building subjected to the impact of discontinuous terrain deformations, in particular sinkholes. The analyses performed allowed for both qualitative and quantitative assessment of the risk of damage. The qualitative assessment allowed for indicating potential locations of structural damage, while the stresses occurring in the calculation model assessed the state of risk to the safety of users.

The analysis was carried out for an actual building located in an area covered by historical mining activity dating back to the early 19th century. The shallowest seam was mined at a depth of 20 m below ground level, and the deepest at about 280 m after the building was constructed. The building was erected in the early 1980s after ground deformations caused by earlier mining operations were revealed. It was designed and constructed following recommendations for construction in mining areas exposed to continuous deformations. The last documented mining impacts occurred in 1985 and did not cause damage to the building. The mine was closed in 1999, and in the following years, maintenance of the excavations, including pumping water, was discontinued. As a result of the liquidation of the groundwater depression cone, changes in the ground and water conditions in the subsurface layers occurred, which caused the appearance of sinkholes in the years 2020-2023 near the building. This phenomenon became the basis for the analysis of the predicted behaviour of the building, taking into account the possibility of a sinkhole appearing under the foundations of the building.

The proposed approach introduces a new quality to numerical analyses using the Finite Element Method, taking into account subsurface sinkholes forming beneath the structure. Such analyses are significantly lacking, and their implementation would allow for a better understanding of the mechanisms of structural damage and failure.

The numerical analysis was deterministic and considered the structure's interaction with the ground. The model included all relevant structural elements and the influence of vertical ground displacements caused by the sinkhole. Two scenarios were analysed in which the sinkholes were located in different locations relative to the building.

The results showed that the building would tilt due to partial loss of foundation support, with maximum vertical displacements of about 30 mm. Depending on the location of the sinkhole, the structure showed different tilt patterns: in the first case, the tilt occurred obliquely (NE-SW, Fig. 9), while in the second case, the greatest displacements occurred on the northern wall, causing a tilt in the N-S direction (Fig. 13). This gave a ceiling inclination of 2.0‰ (case 1) and 2.6‰ (case 2). The currently non-binding standard (PN-76/8841-22) allowed a deviation of up to 5 mm on a 2.0 m long levelling rod, which gives 2.5‰ of permissible inclination.

Redistribution of stresses in the ground was also observed (Figs. 10 and 14). As the sinkhole developed, the vertical stresses (σ_{zz}) moved outwards, which resulted in their reduction at the edge of the sinkhole and concentration at a certain distance, where further deformation of the ground was limited. In both cases, in the final phase of calculations, the stresses in the ground under the building did not exceed 120 kPa.

The main tensile stresses (σ_{max}, Figs. 11 and 15) indicate the possibility of crack formation. The areas of the structure where cracks may occur were determined (Figs. 12 and 16). In both cases, scratches appear in places resulting from the nature of the object's operation (cantilever work – case 1 and beam work – case 2) and occur in places where the structure of window and door openings is weakened. Masonry and concrete elements show much greater susceptibility to cracking, whereas in reinforced concrete elements the tensile load-bearing capacity was not exceeded.

As a result of the analysis carried out, it can be concluded that under the presented conditions, the building will not be destroyed as a result of the formation of a sinkhole. The expected damage includes slope and cracking, but these will not exceed the load-bearing capacity of the structure. However, the deterministic nature of the analysis is a limitation, as uncertainties related to soil properties, building characteristics, sinkhole geometry, and modelling methods can all affect the results. The application of probabilistic methods to the analysis of this particular

case is a burdensome undertaking and is only feasible to a limited extent. Future studies should consider using such an approach to better account for these uncertainties.

Moreover, although the obtained results refer to a specific building and geotechnical conditions, the applied methodology and conclusions can guide similar cases. The approach used in this study can be adapted to assess the behaviour of other similar structures in areas threatened by discontinuous ground deformations. To generalise the results, the analysed case should be a starting point for creating a database of similar cases, which would allow for reducing the number of uncertainties and indicate the direction of further research. In each case, however, the influence of variable parameters of sinkholes on the accuracy of geotechnical risk forecasts should be taken into account, which will contribute to a better representation of real conditions.

Acknowledgements

This work was carried out with the support of the Silesian University of Technology, Grant No. BK-211/RB6/2023, and cooperation with the Mine Restructuring Company joint-stock company (SRK S.A.) as part of work no. NB-157/RB6/2023.

References

[1] M. Chudek, Mechanika górotworu z podstawami zarządzania ochroną środowiska w obszarach górniczych i pogórniczych. Publ House Silesian Univ Technol., Gliwice (2010) (in Polish).

[2] P. Strzałkowski, Zarys ochrony terenów górniczych. Publ. House Silesian Univ. Technol., Gliwice (2010) (in Polish).

[3] H. Kratzsch, Mining Subsidence Engineering. Springer-Verlag. Berlin, Heidelberg, New York (1983).

[4] SS. Peng, Coal Mine Ground Control, 3rd ed.; West Virginia University: Morgantown, WV, USA, (2008).

[5] S. Knothe, Prognozowanie wpływów eksploatacji górniczej. Wydawnictwo Śląsk, Katowice (1984) (in Polish).

[6] B.W. Whittaker, D.J. Reddish, Subsidence – Occurrence, Prediction and Control. Elsevier, Amsterdam-Oxford-New York-Tokyo (1989).

[7] K. Tajduś, Numerical Simulation of Underground Mining Exploitation Influence Upon Terrain Surface. Archives of Mining Sciences **58** (3), 605-616 (2013). DOI: https://doi.org/10.2478/amsc-2013-0042

[8] K. Tajduś, Analysis of horizontal displacement distribution caused by single advancing longwall panel excavation. Journal of Rock Mechanics and Geotechnical Engineering **7**, 4, 395-403 (2015). DOI: https://doi.org/10.1016/j.jrmge.2015.03.012

[9] M. Wesołowski, Numerical modelling of exploitation relics and faults influence on rock mass deformations. Archives of Mining Sciences **61**, 4, 893-906 (2016). DOI: https://doi.org/10.1515/amsc-2016-0059

[10] B. Ghabraie, G. Ren, J. Barbato, J. Smith, A predictive methodology for multi mining induced subsidence. International Journal of Coal Geology Elsevier **93**, 280-294 (2017). DOI: https://doi.org/10.1016/j.ijrmms.2017.02.003

[11] J. Blachowski, S. Cacoń, W. Milczarek, Analysis of post-mining ground deformations caused by underground coal extraction in complicated geological conditions. Acta Geodyn. Geomater. **6**, 351-357 (2009).

[12] X. Lian, H. Hu, Terrestrial laser scanning monitoring and spatial analysis of ground disaster in Gaoyang coal mine in Shanxi, China: a technical note. Environ. Earth Sci. **76**, 287 (2017). DOI: https://doi.org/10.1007/s12665-017-6609-6

[13] P. Strzałkowski, Predicting mining areas deformations under the condition of high strength and depth of cover. Energies **15**, 1-17 (2022). DOI: https://doi.org/10.3390/en15134627

[14] W. Piwowarski, B. Dżegniuk, Z. Niedojadało, Współczesne teorie ruchów górotworu i ich zastosowanie. Wydawnictwo AGH, Kraków (1995) (in Polish).

[15] E. Popiołek, Ochrona terenów górniczych. Wyd. AGH, Kraków (2009) (in Polish).

[16] R. Misa, K. Tajduś, A. Sroka, Impact of geotechnical barrier modelled in the vicinity of a building structures located in mining area. Arch. Min. Sci. **63**, 4, 919-933 (2018). DOI: https://doi.org/10.24425/ams.2018.124984

[17] A. Sroka, R. Misa, K. Tajduś, M. Dudek, Analytical design of selected geotechnical solutions which protect civil structures from the effects of underground mining. Journal of Sustainable Mining **18**, 1, 1-72 (2019). DOI: https://doi.org/10.1016/j.jsm.2018.10.002

[18] M. Kawulok, Szkody górnicze w budownictwie. Instytut Techniki Budowlanej, Warszawa (2015) (in Polish).

[19] L. Chomacki, J. Rusek, L. Słowik, Selected Artificial Intelligence Methods in the Risk Analysis of Damage to Masonry Buildings Subject to Long-Term Underground Mining Exploitation. Minerals **11** (9), 958 (2021). DOI: https://doi.org/10.3390/min11090958

[20] L. Chomacki, J. Rusek, L. Słowik, Machine Learning Methods in Damage Prediction of Masonry Development Exposed to the Industrial Environment of Mines. Engineers **15** (11), 3985 (2022). DOI: https://doi.org/10.3390/en15113958

[21] J. Kwiatek, Protection of construction objects in mining areas. Publishing House of Central Mining Institute, Katowice (1997) (in Polish).

[22] L. Szojda, Numerical analysis of the influence of non-continuous ground displacement on masonry structure. Silesian University of Technology Publishing House, Monograph, Gliwice (2009) (in Polish).

[23] D. Mrozek, M. Mrozek, J. Fedorowicz, The protection of masonry buildings in a mining area. Procedia Engineering 193 International Conference on Analytical Models and New Concepts in Concrete and Masonry Structures AMCM'2017: 184-191. Gliwice (2017). DOI: https://doi.org/10.1016/j.proeng.2017.06.202

[24] M. Abdallah, T. Verdel, Behaviour of a masonry wall subjected to mining subsidence, as analysed by experimental designs and response surfaces. International Journal of Rock Mechanics and Mining Sciences **100**, 199-206 (2017). DOI: https://doi.org/10.1016/j.ijrmms.2017.10.003

[25] L. Szojda, Ł. Kapusta, Evaluation of the elastic model of a building on a curved mining ground based on the result of geodetic monitoring. Archives of Mining Sciences **65** (2), 213-224 (2020).

DOI: https://doi.org/10.24425/ams.2020.133188

[26] Instrukcja Instytutu Techniki Budowlanej nr 364/2007: Wymagania techniczne dla obiektów budowlanych wznoszonych na terenach górniczych. Wydawnictwo ITB, Warszawa (2007) (in Polish).

[27] Instrukcja Instytutu Techniki Budowlanej nr 416/2006: Projektowania budynków na terenach górniczych. Wydawnictwo ITB, Warszawa (2006) (in Polish).

[28] M. Chudek, W. Janusz, J. Zych, Studium dotyczące stanu rozpoznania tworzenia się i prognozowania deformacji nieciągłych pod wpływem podziemnej eksploatacji złóż. Zeszyty Naukowe Politechniki Śląskiej, seria Górnictwo, 141, Gliwice (1988) (in Polish).

[29] P. Strzałkowski Sinkhole formation hazard assessment. Environ. Earth Sci. **78**, 1–6 (2019). DOI: https://doi.org/10.1007/s12665-018-8002-5

[30] K. Kuźniar, T. Tatara, SSI Effect in Two Mining Regions for Low-Rise Traditional Buildings. Mechanisms and Machine Science **125**, 337-344 (2023). DOI: https://doi.org/10.3390/en15238963

[31] K. Kuźniar, T. Tatara, The ratio of response spectra from seismic-type free-field and building foundation vibrations: the influence of rockburst parameters and simple models of kinematic soil-structure interaction. Bulletin of Earthquake Engineering **18**, 907-924 (2020). DOI: https://doi.org/10.1007/s10518-019-00734-w

[32] Rozporządzenie Parlamentu Europejskiego i Rady (UE) 2021/1119 z dnia 30.06.2021 r. w sprawie ustanowienia ram na potrzeby osiągnięcia neutralności klimatycznej i zmiany rozporządzeń (WE) nr 401/2009 i (UE) 2018/1999 (Europejskie prawo o klimacie) (in Polish).

[33] X. Li, S.J. Wang, T.Y. Liu, F.S. Ma, Engineering geology, ground surface movement and fissures induced by underground mining in the Jinchuan Nickel Mine. Engineering Geology **76**, 1-2, 93-107 (2004). DOI: https://doi.org/10.1016/j.enggeo.2004.06.008

[34] K. Woo, E. Eberhardt, D. Elmo, D. Stead, Empirical investigation and characterisation of surface subsidence related to block cave mining. International Journal of Rock Mechanics and Mining Science **61**, 31-42 (2013). DOI: https://doi.org/10.1016/j.ijrmms. 2013.01.01

[35] R. Ścigała, Wpływ tektoniki złoża na rozkład deformacji terenu górniczego. Wyd. Pol. Śl. Gliwice (2013) (in Polish).

[36] A. Frolik, J. Kubica, Ocena stanu zagrożenia wodnego i jego ryzyka w kopalnia węgla kamiennego. Research Report Central Mining Institute, Mining and Environment Quarterly **4**, 61-76 (2005).

[37] P. Bukowski, Evaluation of Water Hazard in Hard Coal Mines in Changing Conditions of Functioning of Mining Industry in Upper Silesian Coal Basin-USCB (Poland). Archives of Mining Sciences **60**, 2, 455-475 (2015). DOI: https://doi.org/10.1515/amsc-2015-0030

[38] Dokumentacja z wykonania robót likwidacyjno-zabezpieczających pn. „Naprawa szkód polegająca na przywróceniu stanu poprzedniego poprzez likwidację zagrożenia powstaniem deformacji nieciągłych na nieruchomości (…)". EKOWIERT sp. z o.o. Katowice ul. Dunikowskiego 12-14.12.2014 r. (in Polish).

[39] Z. Wiłun, Zarys geotechniki. Wydawnictwa Komunikacji i Łączności. Warszawa (1987) (in Polish).

[40] V. Červenka, L. Jendele, J. Červenka, ATENA Program Documentation – Part 1: Theory, Prague, (2018).

[41] D. C. Drucker, W. Prager, Soil mechanics and plastic analysis for limit design. Quarterly of Applied Mathematics **10**, 2, 157-165 (1952).

[42] B. Đurin, M. Kancijan, A. Aniskin, B. Soldo D. C. Drucker, W. Prager, The current state of soil mechanics models. e-ZBIORNIK, Electronic collection of papers of the Faculty of Civil Engineering **12**, 24, 12-28 (2022). DOI: https://doi.org/10.47960/2232-9080.2022.24.12.12.

[43] K.J. Willam, E.P. Warnke, Constitutive Model for the Triaxial Behavior of Concrete. Proceedings of IABSE, Structural Engineering Report 19, Section III, pp. 1-30, (1975).

[44] H. Sjøl, Material models for concreto exposed to impact loading. Norwegian Defence Research Establishment, FFI Raport 23/00669, (2023), ISBN 978-82-464-3479-7.

[45] S. Majewski, L. Szojda, Modelling of masonry structures by FEM, W: Analytical models and new concepts in concrete and masonry structures: 4th International conference. AMCM 2002, Kraków, June 5th-7th 2002. Conference proceedings, 2002, Kontekst Publisher, s. 207-212.

[46] L. Szojda, Numerical analysis of masonry structures, Proceedings of the Eighth International Masonry Conference held in Dresden from 4th to 7th of July 2010: Masonry (11): Vol. 2, Proceedings of the British Masonry Society, vol. 11, 2010, International Masonry Society, ISBN 978-3-00-031381-3, s. 1009-1017.

[47] Collective work, Editors: E. Pliszek, E. Krzemińska-Niemiec, Poradnik inżyniera i technika budowlanego, Vol. 2, Part II, Warszawa 1969 (in Polish).

[48] R. Jasiński, K. Grzyb, Proposal of Empirical Homogenization Of Masonry Wall Made of AAC Masonry Units. IOP Conference Series: Materials Science and Engineering **960**, 2, (2020).

[49] P. Matysek, „Identyfikacja wytrzymałości na ściskanie i odkształcalności murów ceglanych w obiektach istniejących", Kraków 2014 (in Polish).